

Relaxation dynamics of vortex lines in disordered type-II superconductors following magnetic field and temperature quenches

Hiba Assi¹, Harshwardhan Chaturvedi¹, Ulrich Dobramysl², Michel Pleimling¹, and Uwe C. Täuber¹

¹*Department of Physics (MC 0435), 850 West Campus Drive, Virginia Tech, Blacksburg, Virginia 24061 and*

²*Mathematical Institute, University of Oxford, Andrew Wiles Building, Radcliffe Observatory Quarter, Woodstock Road, Oxford OX2 6GG, U.K.*

(Dated: June 10, 2019)

We study the effects of rapid temperature and magnetic field changes on the non-equilibrium relaxation dynamics of magnetic vortex lines in disordered type-II superconductors by employing an elastic line model and performing Langevin molecular dynamics simulations. In a previously equilibrated system, either the temperature is suddenly changed, or the magnetic field is instantaneously altered which is reflected in adding or removing flux lines to or from the system. The subsequent aging properties are investigated in samples with either randomly distributed point-like or extended columnar defects, which allows to distinguish the complex relaxation features that result from either type of pinning centers. One-time observables such as the radius of gyration and the fraction of pinned line elements are employed to characterize steady-state properties, and two-time correlation functions such as the vortex line height autocorrelations and their mean-square displacement are analyzed to study the non-linear stochastic relaxation dynamics in the aging regime.

PACS numbers: 05.40.-a, 74.25.Wx, 74.25.Uv, 74.40.-n, 74.62.En

I. INTRODUCTION

Type-II superconductors have been the focus of many theoretical and experimental investigations since their discovery. From the fundamental physics perspective, these materials represent a class of systems with many competing energy scales and thus a remarkably rich variety of thermodynamic phases, as well as intriguingly complex transport properties [1]. Applied science and engineering research on type-II superconductors has focused primarily on their optimization for technological applications, especially in magnetic fields. The most prominent desirable property of superconductors is of course the absence of current flow dissipation in these materials. However in the mixed phase of type-II superconductors, magnetic flux enters the sample in the form of quantized vortex lines, and external driving currents generate a Lorentz force that in turn causes these vortices to move, creating Ohmic dissipation in the system. To prevent flux flow and thus restore dissipation-free transport, effective pinning mechanisms of flux lines to material defects are required [1].

Different types of defects are utilized as pinning centers for magnetic vortices, predominantly uncorrelated point-like disorder and extended linear (columnar) defects. Point defects are naturally occurring, e.g., in ceramic high- T_c materials in the form of oxygen vacancies, but can also be artificially introduced, for instance by electron irradiation [2]. The presence of weak point pinning centers destroys the long-range crystalline order of the low-temperature Abrikosov flux line lattice in the disorder-free system, to form either a genuine disordered vortex glass phase [3–7] or a Bragg glass state that is characterized by quasi long-range positional order [8–13]. The thermally induced first-order melting transition of the vortex lattice at elevated temperatures [14–16] is

thereby replaced by a disorder-driven continuous phase transition between frustrated ('glassy') low-temperature states and a fluctuating flux liquid phase.

Columnar defects too may be naturally present in the sample as line dislocations, and can in addition be artificially introduced by growing them using, for instance, MgO nanorods [17] or through irradiating the sample with high-energy ions such as Sn, Pb, or Iodine. In contrast with point-like disorder, the presence of correlated columnar defects results in the emergence of a novel low-temperature thermodynamic state distinct from the vortex glass phase, namely the strongly pinned Bose glass [7, 18–21]. Since vortex lines become then localized along the entire length of these linear pinning centers, the sample's tilt modulus diverges (transverse Meissner effect) [20, 22]. Indeed, columnar defects have experimentally proven more efficient at pinning than uncorrelated point-like disorder due to their extended nature [23].

We emphasize that in the vortex glass phase in the presence of point-like disorder, the low-energy flux line contours tend to roughen as the vortices minimize their free energy in the disordered pinning landscape, while in the Bose glass phase in the presence of columnar defects that are oriented along the magnetic field direction the bound vortex lines are effectively straight. Therefore, these two disorder-dominated glassy phases in fact display very different lateral and transverse vortex line fluctuations. One consequently expects samples with point disorder and columnar defects to yield profoundly distinct non-equilibrium relaxation properties.

Some materials undergo slow relaxation processes to eventually reach thermal equilibrium, which affects their measured dynamical properties and renders these effectively time-dependent; this is referred to as physical 'aging' [24, 25]. Many glassy systems have been observed to undergo physical aging [26] owing to the very slow

kinetics between a large number of energetically close metastable states typically emerging in frustrated environments. In a superconducting 2H-NbSe₂ sample, Du *et al.* discovered that the voltage response to an applied current pulse depended on the pulse duration [27], which constitutes clear evidence of physical aging in disordered vortex matter. Papadopoulou *et al.* observed aging effects in the measurement of the zero-field cooled magnetization in the compound Bi₂Sr₂CaCu₂O₈ [28].

On the numerical front, Bustingorry, Cugliandolo, and Domínguez pioneered Langevin molecular dynamics simulations of a three-dimensional model of vortex matter to identify physical aging features in certain two-time correlation functions [29, 30]. Pleimling and Täuber then employed an elastic line model and Monte Carlo simulations to study the non-equilibrium relaxation properties of magnetic vortices in type-II superconductors starting from somewhat artificial initial configurations where straight flux lines were placed at random positions in the sample [31]. The resulting complex aging features (with identical initial conditions and parameter values) were subsequently confirmed in a very different microscopic representation of the non-equilibrium vortex kinetics through Langevin molecular dynamics [32].

In this present work, we investigate in detail the aging relaxation dynamics of vortex matter in disordered type-II superconductors starting from experimentally realizable initial conditions, where we analyze the effects of sudden changes in either the system's ambient temperature or magnetic field. This allows us to both make closer contact to experiment, and to explicitly test the sensitivity of the non-equilibrium aging kinetics to the selection of initial states. As in our earlier studies, we can switch off the repulsive vortex interactions, the pinning potentials, or both in our computer simulations, and thereby identify the physical mechanisms for the observed complex features in the vortex relaxation dynamics. Again, crucial differences in the fluctuation spectrum for vortex matter in the presence of point-like or extended defects become apparent. In addition, separately tracking the behavior of the originally present, already relaxed flux lines and the newly added vortices helps our analysis of the simulations with sudden magnetic field increases.

One of the principal goals of this investigation is to identify observable correlations that allow a dynamical characterization of material samples. Experimental methods that could be used to extract the relevant quantities include the following techniques: Vortices in type-II superconductors were imaged by Vasyukov *et al.* using nano-SQUIDs in scanning probe microscopy [33], with recorded magnetic fields down to 50 nT. Furthermore, Auslaender *et al.* used the tip of a magnetic force microscope to drag the end of a single vortex across the surface of a YBCO sample, directly measuring its interaction with a local disorder potential, in order to study the dynamics of vortices and their (de-)pinning processes from different defects [34]. Flux creep parameters in YBCO samples were experimentally investigated by Abulafia *et*

al. by utilizing an array of microscopic Hall sensors [35]. These methods could perhaps be utilized to probe the relaxation processes of magnetic vortex lines in a disordered medium following quenches in temperature or magnetic field, and to distinguish the effects of different types of disorder on the dynamics of this complex system.

This paper is organized as follows: In the next section, we describe the elastic line model and the Langevin molecular dynamics simulation algorithm that we employ in our study, and also specify the material parameters that we use in our computational model. Then, we specify the single-time quantities and two-time correlation functions that are measured in our simulations to analyze the non-equilibrium and aging properties of our vortex matter models. The last part of this section is devoted to a discussion of finite-size effects and a verification that our numerical results are not specific to the system size we choose. Section III discusses the effects of temperature quenches on the relaxation properties in systems of interacting flux lines subject to either point-like or columnar disorder. In Section IV, we present the relaxation dynamics in the aging regime following magnetic field quenches. We compare the effects of sudden increases or decreases of the vortex density to our earlier studies where the magnetic field remained fixed. We systematically disentangle the contributions due to repulsive vortex interactions and pinning to disorder. We find the non-equilibrium relaxation features of vortex matter to strongly depend on the type of disorder present in the system. We finally summarize our work in the concluding Section V.

II. MODEL DESCRIPTION AND SIMULATION PROTOCOL

A. Elastic Line Description

In the following numerical study, we consider systems composed of N vortex lines in the extreme London limit, where the London penetration depth λ is much larger than the coherence length ξ , which allows us to employ a fully three-dimensional elastic line description [20, 36]. The vortices are described through their trajectories $\vec{r}_i(z)$, *i.e.*, their two-dimensional *ab* plane position vectors as function of the z coordinate along the direction of the applied external magnetic field. The system's Hamiltonian can then be written as a functional of the N interacting trajectories $\vec{r}_i(z)$:

$$H[\vec{r}_i] = \sum_{i=1}^N \int_0^L dz \left[\frac{\tilde{\epsilon}_1}{2} \left| \frac{d\vec{r}_i(z)}{dz} \right|^2 + U_D(\vec{r}_i(z), z) \right. \\ \left. + \frac{1}{2} \sum_{j \neq i}^N V(|\vec{r}_i(z) - \vec{r}_j(z)|) \right]. \quad (1)$$

This effective free energy consists of three competing terms: the elastic vortex line tension, an attrac-

tive potential describing the N_D pinning centers, and the repulsive interactions between different vortices. The elastic line stiffness or local tilt modulus is given by $\tilde{\epsilon}_1 \approx \Gamma^{-2} \epsilon_0 \ln(\lambda_{ab}/\xi_{ab})$, where $\Gamma^{-1} = M_{ab}/M_c$ is the anisotropy parameter (effective mass ratio). λ_{ab} and ξ_{ab} respectively denote the London penetration depth and the coherence length in the ab crystallographic plane. Moreover, the in-plane vortex repulsive interactions are given by $V(r) = 2\epsilon_0 K_0(r/\lambda_{ab})$, with K_0 denoting the zeroth-order modified Bessel function, which essentially represents a logarithmic repulsion that is exponentially screened at the scale λ . We set a cut-off for the interactions in our simulations at $5\lambda_{ab}$ to avoid artifacts due to the periodic boundary conditions.

We discretize the Hamiltonian (1) in the z direction, and model N_D point-like pinning centers as spatially randomly distributed smooth potential wells of the form

$$U_D(\vec{r}, z) = -\sum_{\alpha=1}^{N_D} \frac{b_0}{2} p \delta(z - z_\alpha) \left[1 - \tanh \left(5 \frac{|\vec{r} - \vec{r}_\alpha| - b_0}{b_0} \right) \right], \quad (2)$$

where \vec{r}_α and z_α respectively denote the in-plane and z coordinates of pinning center α , and $p \geq 0$ represents the pinning potential strength. Columnar defects are set up by first randomly selecting the in-plane coordinates \vec{r}_α , and then placing identical potential wells (2) at all z positions z_α . Henceforth, all lengths are measured relative to the pinning potential width b_0 , and energies are measured in units of $\epsilon_0 b_0$ with $\epsilon_0 = (\phi_0/4\pi\lambda_{ab})^2$, where $\phi_0 = hc/2e$ is the magnetic flux quantum.

B. Langevin Molecular Dynamics

We analyze the vortex kinetics by means of a Langevin molecular dynamics algorithm. As mentioned above, we discretize space in the z direction (along the external magnetic field) into layers, whose spacing corresponds to the unit cell size c_0 along the crystal's c direction [36, 37]. The effective forces acting on each flux line element are then computed as spatial derivatives of the discretized version of the Hamiltonian (1). Correspondingly, we discretize and numerically solve the overdamped Langevin equation

$$\eta \frac{\partial \vec{r}_i(t, z)}{\partial t} = -\frac{\delta H[\vec{r}_i(t, z)]}{\delta \vec{r}_i(t, z)} + \vec{f}_i(t, z), \quad (3)$$

with the Bardeen-Stephen viscous drag parameter η by direct temporal integration [38]. Note that all fast degrees of freedom (*e.g.*, phonons etc.) are captured by thermal stochastic forces, which are modeled as uncorrelated Gaussian white noise with vanishing mean $\langle \vec{f}_i(t, z) \rangle = 0$. We impose the Einstein relation

$$\langle \vec{f}_i(t, z) \vec{f}_j(s, z') \rangle = 2\eta k_B T \delta_{ij} \delta(t - s) \delta(z - z') \quad (4)$$

to guarantee that the system asymptotically reaches thermal equilibrium with a canonical probability distribution $\propto e^{-H/k_B T}$.

C. Material Parameters

We select our material parameters guided by the actual values for the ceramic high- T_c type-II superconducting compound $\text{YBa}_2\text{Cu}_3\text{O}_7$ (YBCO). All simulation distances are measured in units of the pinning center radius, which we set to $b_0 = 35\text{\AA}$. We choose the spacing between layers in the c direction equal to this basic microscopic scale, $c_0 = b_0$. The in-plane London penetration depth is $\lambda_{ab} = 34b_0 \approx 1200\text{\AA}$, and the superconducting coherence length $\xi_{ab} = 0.3b_0 \approx 10.5\text{\AA}$. This emulates the high anisotropy of YBCO, with an effective mass anisotropy ratio $\Gamma^{-1} = 1/5$. All simulation energies are measured in units of $\epsilon_0 b_0$, where ϵ_0 is the line energy per unit length: $\epsilon_0 \approx 1.92 \cdot 10^{-6} \text{ erg/cm}$. The vortex line tension energy scale becomes $\tilde{\epsilon}_1/\epsilon_0 \approx 0.189$. The depth of the pinning potential wells is fixed at $p/\epsilon_0 = 0.05$. We perform our numerical runs at temperatures $T = 10 \dots 40 \text{ K}$, with $T = 10 \text{ K}$ corresponding to $k_B T/\epsilon_0 b_0 = 0.002$ in our simulation units. Finally, we set the Bardeen-Stephen viscous drag coefficient $\eta = \phi_0^2/2\pi\rho_n c^2 \xi_{ab}^2 \approx 10^{-10} \text{ erg} \cdot \text{s} / \text{cm}^2$ to one (for the normal-state resistivity of YBCO near T_c , $\rho_n \approx 500 \mu\Omega \text{ cm}$, see Table 1 in Ref. [39]); thus the simulation time steps are fixed by the fundamental temporal unit $t_0 = \eta b_0/\epsilon_0 \approx 18 \text{ ps}$. In the following, all times are measured in simulation time steps, i.e., in units of t_0 .

D. Simulation Protocol

Our aim is to impose experimentally realizable initial conditions to bridge theoretical simulations and experimental work. To this end, we investigate sudden changes in the magnetic field or temperature. A magnetic field quench is implemented in our simulations by adding flux lines at random positions in the system (up-quench) or removing randomly selected vortices from the system (down-quench). We start with straight flux lines positioned at random in the sample, and let the system relax up to an initial relaxation time $r = 10^5$. We then instantaneously increase the magnetic field by adding 5 straight flux lines to the 16 originally present and essentially relaxed vortices; or instantaneously decrease the field by removing 5 random lines from 21 relaxed initial vortices. Subsequently, we let the resulting system relax up to a waiting time s , at which a snapshot of the system is taken; the waiting time s is measured after the quench. At later times $t > s$, different two-time correlation functions are evaluated. Since r is much larger than the different waiting times s and measurement time t , it is crucial to take this elapsed time period into account when considering the initial lines that have relaxed for a dura-

tion r . We therefore introduce the times $\sigma = r + s$ and $\Gamma = r + t$. Temperature quenches are accomplished by letting the initial configuration of $N = 16$ flux lines relax up to a similar initial relaxation time ($t = 10^5$) at which the temperature is suddenly raised or lowered. Throughout our analysis of magnetic field and temperature quenches, the number of layers is $L = 640$ and the number of pinning sites per layer is fixed at $N_D/L = 1710$.

E. Measured Quantities

We measure various two-time correlation functions, some of which provide insight into the local features of the fluctuating vortex lines, such as their *height-height autocorrelations*

$$C(t, s) = \langle [\vec{r}_{i,z}(t) - \bar{\vec{r}}_i(t)] [(\vec{r}_{i,z}(s) - \bar{\vec{r}}_i(s))] \rangle, \quad (5)$$

where $\vec{r}_{i,z}(t)$ are the in-plane coordinates of line i at layer z at time t , and $\bar{\vec{r}}_i(t) = \langle \vec{r}_{i,z}(t) \rangle$ is the mean lateral position of line i at time t . These are averaged over all line elements and over many noise histories and disorder realizations. $C(t, s)$ thus measures the thermal fluctuations of line elements around their corresponding mean lateral line position.

The global structure of the flux line configuration is analyzed using the two-time *mean-square displacement*

$$B(t, s) = \langle [\vec{r}_{i,z}(t) - \vec{r}_{i,z}(s)]^2 \rangle. \quad (6)$$

This correlation function measures the average square distance between the position of a line element at time s and the position of that same line element at a later time t . Both two-time correlation functions were also analyzed in Refs. [31] and [32], where Monte Carlo and Langevin molecular dynamics simulations, respectively, were performed to characterize the complex non-equilibrium relaxation of initially straight and randomly placed vortex lines in the presence of point-like disorder. Thermal spatial fluctuations can also be quantified by means of the vortex line radius of gyration

$$r_g(t) = \sqrt{\langle [\vec{r}_{i,z}(t) - \bar{\vec{r}}_i(t)]^2 \rangle}, \quad (7)$$

i.e., the root mean-square displacement from the lines' mean lateral position at time t .

Another one-time observable that we measure in our simulations is the fraction $\varphi(t)$ of pinned line elements when disorder is present. To this end, we first find the number of line elements that reside within a fixed small cut-off distance from a certain pinning center at a given time t . Then we divide this count by the total number of line elements present in the sample to yield $\varphi(t)$. Throughout our study, the cut-off distance is set equal to the pinning center radius, $r_c = b_0$. The total number of line elements can be computed by multiplying the number of layers $L = 640$ in the z direction with the number N of vortex lines present in the system.

F. Finite-Size Effects

In our work, we restrict ourselves to a low magnetic field or vortex density regime, and only consider systems composed of between $N = 10$ and $N = 21$ vortices. This naturally constitutes a tiny system compared to typical experimental samples of disordered type-II superconductors in external magnetic fields. It is therefore crucial to analyze the effects of this small vortex density, especially when we remove lines as the magnetic field sudden decreases. We consequently ran simulations in systems with different numbers of flux lines, but keeping the density of pinning centers the same in all cases.

As demonstrated in Fig. 1, the data for the vortex radius of gyration $r_g(t)$, mean-square displacement $B(t, 0)$, and the fraction $\varphi(t)$ of pinned line elements that correspond to systems of different number of flux lines col-

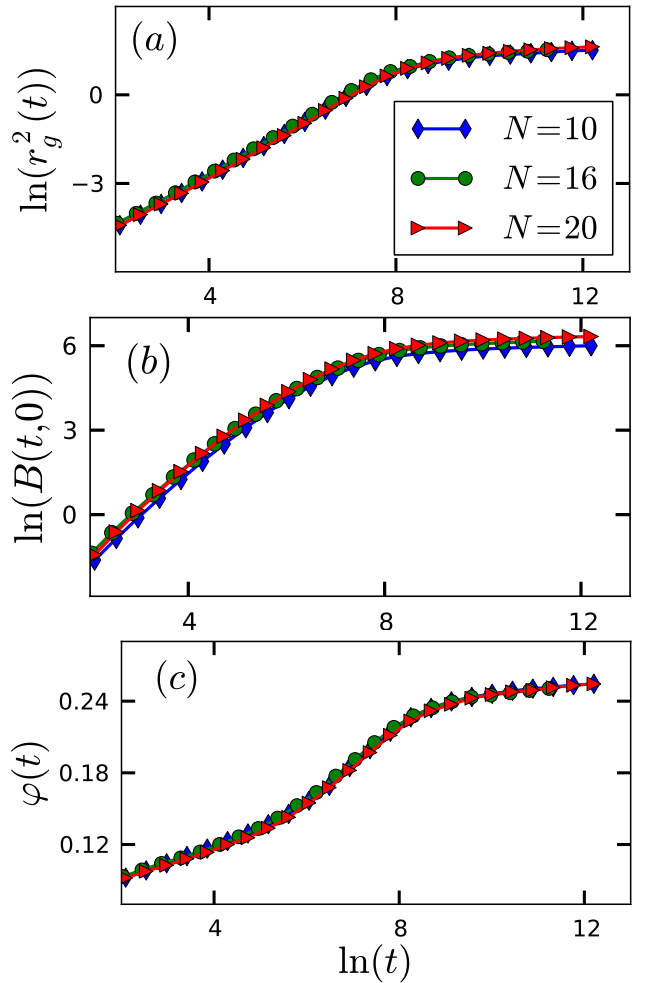


FIG. 1: (Color online) Relaxation of the (a) gyration radius, (b) mean-square displacement, and (c) fraction of pinned line elements for (dilute) systems with different number of interacting vortex lines in the presence of point-like pinning centers, averaged over 100 disorder and noise realizations.

lapse onto a common curve. Therefore, we conclude that these differently-sized systems follow similar relaxation processes confirming that finite-size effects do not play a prominent role in this computational study of dilute systems of flux lines in a dissipative medium. It is worth noting that the physics in denser vortex systems could of course be quite different.

III. TEMPERATURE QUENCHES

We first consider sudden changes in the ambient temperature, with the goal to analyze the effects of instantaneous increases in temperature on the system's relaxation dynamics. At $t = 10^5$ in our simulation, we instantaneously increase the temperature from $T = 0.002$ to $T = 0.008$ in a system of $N = 16$ interacting flux lines in the presence of either point or columnar pinning centers. We then compare the relaxation of the radius of gyration $r_g(t)$ and the fraction of pinned line elements $\varphi(t)$ when the temperature stays fixed with the scenario wherein it is suddenly raised. We remark that the error bars displayed in some of the figures in this section, however small they appear, always represent the standard error of the mean of the computed quantities. We observe that the relaxation of these observables in the considered systems can invariably be mapped to an exponential function of the form $a e^{-t/\tau} + c$, where τ determines a characteristic relaxation time. The measured values for the relaxation times τ in different scenarios are summarized in Table I. We note that the exponential relaxation of observables in our vortex model system following sudden temperature quenches implies that physical aging features would not be discernible on time scales larger than the relaxation time τ .

Defect type	$T = 0.002$	$T = 0.008$	$T = 0.002 \rightarrow 0.008$
	r_g		φ
(a) Point-like	$5.9 \cdot 10^4$	$5.3 \cdot 10^4$	$3.5 \cdot 10^4$
(b) Columnar	$3.5 \cdot 10^4$	$4.9 \cdot 10^4$	$\tau_1 = 1.6 \cdot 10^3$ $\tau_2 = 5.7 \cdot 10^4$

TABLE I: Measured characteristic relaxation times for the gyration radius r_g and the fraction of pinned line elements φ in systems of interacting vortex lines with (a) point-like and (b) columnar defects (data averaged over 1000 realizations).

In systems with point-like disorder, the measured relaxation time of the radius of gyration at high temperature is shorter than that at low temperature, see Table I. This confirms that thermal fluctuations facilitate the roughening of vortices in the presence of point-like disorder. Following a sudden increase in temperature, the radius of gyration first decreases a little as a few flux line segments become thermally depinned, and subsequently increases monotonically, as shown in Fig. 2a. We checked that this increase in $r_g(t)$ is well described by an exponential function of the form $a e^{-t/\tau} + c$, with

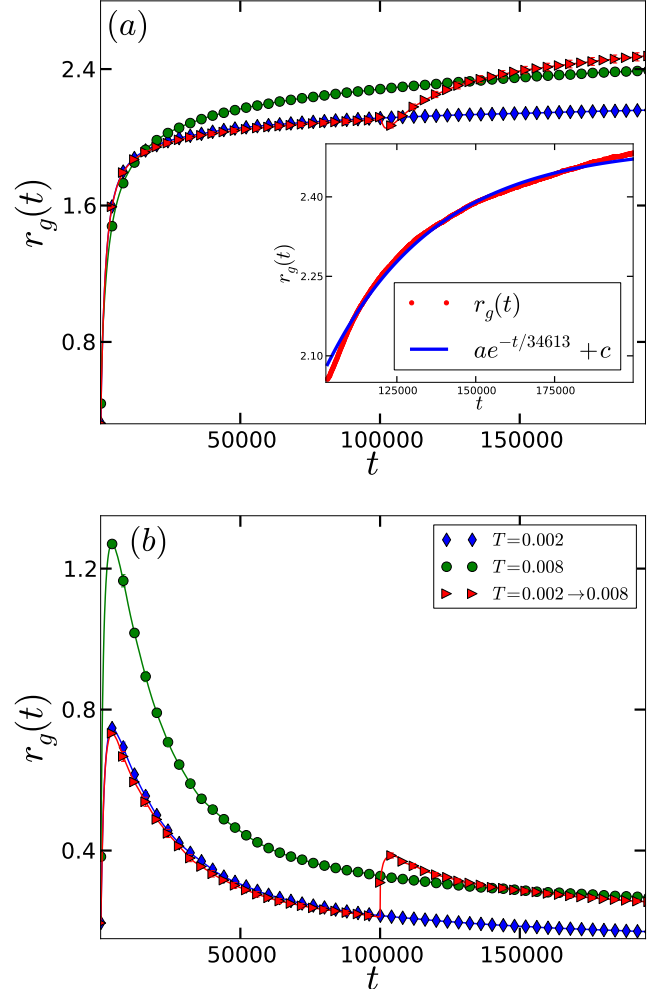


FIG. 2: (Color online) Relaxation of the gyration radius in systems of interacting vortex lines with (a) point disorder or (b) columnar defects, when the temperature is either held fixed or instantaneously raised (data averaged over 1000 realizations). The inset in (a) shows the gyration radius following the sudden temperature increase in the presence of point disorder, and a fit to an exponential function.

relaxation time $\tau = 3.5 \cdot 10^4$ (the other parameters are $a \approx -1.73$ and $c \approx -0.09$) as observed in the inset in Fig. 2a. Thus, as expected, point defects enhance thermal wandering of flux lines in this disordered landscape.

In contrast, systems with columnar defects actually require a longer relaxation time for the radius of gyration at higher temperatures than that at lower temperatures, see Table I, asserting that thermal fluctuations resist the straightening of vortex lines as they become localized at columnar pinning centers. When we instantaneously increase the temperature in this system, the gyration radius after the quench shows a marked fast increase, even beyond the relaxation curve for a system at constant higher temperature, followed by a much slower decrease, see Fig. 2b. The initial increase in r_g can likely be at-

tributed to the creation of double-kinks in the system that are not similarly generated in relaxation processes at fixed temperature, while the final decrease is due to the decay of these metastable configurations. A double-kink refers to a flux line configuration where the vortex is simultaneously pinned to two adjacent columnar defects. This is a long-lived state which will eventually decay to either a free vortex, or, more probably, to a straight flux line bound to a single defect column. We find that both the initial increase and the final decrease in the gyration radius again fit an exponential of the form $a e^{-t/\tau} + c$, but with different relaxation times (and signs of the coefficient a): In Fig. 2b, the fast relaxation time from the initial non-equilibrium steady state at $T = 0.002$ to the metastable state with vortex double-kinks is $\tau_1 = 1.6 \cdot 10^3$, while the much longer relaxation time from this intermediate state to the final non-equilibrium steady state at $T = 0.008$ is $\tau_2 = 5.7 \cdot 10^4$. Note that the data for the gyration radius for both the temperature up-quench scenario as well as at a fixed high temperature in Figs. 2a and 2b will eventually approach the same curve in the long-time limit, which has not yet been reached in our simulation time window.

The differences between the systems' responses to temperature up-quenches in the presence of point and columnar pinning centers, respectively, can be attributed to the very distinct (de-)pinning behavior that we shall again discuss later in the context of sudden magnetic field changes. When the temperature is suddenly raised in systems with uncorrelated point disorder, some line elements become thermally depinned. The vortices are initially straightened owing to their line tension. Subsequently an increasing number of line elements finds favorable pinning sites, causing a monotonic growth in their transverse spatial fluctuations measured by r_g . In samples with columnar defects, following a temperature up-quench some line elements migrate away from certain columnar pinning centers, which renders them subject to thermal wandering. Yet they soon become pinned to neighboring defect lines causing the subsequent decrease in the lateral spatial vortex line fluctuations, akin to systems relaxing at fixed temperature.

This scenario is confirmed by the relaxation data for the fraction of pinned line elements $\varphi(t)$ in Fig. 3. As observed in Fig. 3a, in the presence of point disorder only a minority ($\approx 25\%$) of line elements are actually pinned right before the temperature quench. A sudden increase in temperature releases a significant fraction of these pinned line elements causing a decrease in φ as well as the small dip in r_g . Later, the vortices become attached to and hence stretched between point-like pins causing a subsequent increase in φ , accompanied with a monotonic increase in the lines' spatial fluctuations.

In the presence of columnar defects, on the other hand, Fig. 3b shows that almost all line elements are bound to pinning centers just before the temperature quench is applied. The sudden temperature increase causes a tiny number of these line elements to depin from their

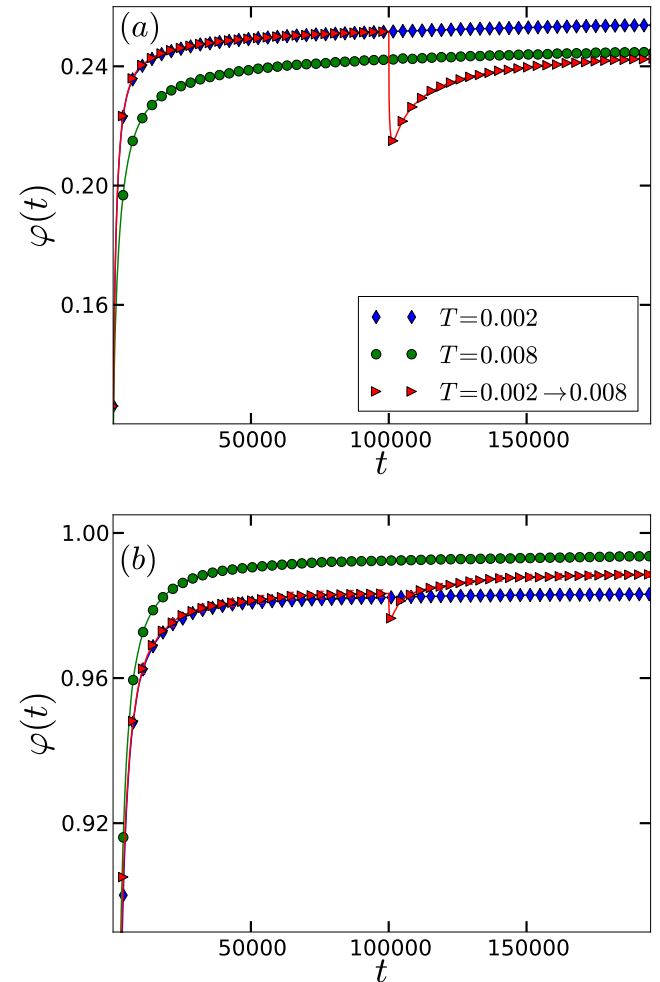


FIG. 3: (Color online) Relaxation of the fraction of pinned line elements in systems of interacting vortex lines with (a) point disorder or (b) columnar defects, when the temperature is either held fixed or instantaneously raised (data averaged over 1000 realizations).

localizing columns. However, they are soon to be pinned again, but partly in metastable double-kink configurations. This explains the non-monotonic pattern we observe in the spatial fluctuations with a rapid increase of r_g followed by a slow decrease. Finally, the fraction of pinned line elements $\varphi(t)$ following the temperature quench in the presence of both types of disorder once again fits an exponential of the form $a e^{-t/\tau} + c$, yet with different relaxation times: $\tau = 3.1 \cdot 10^4$ for point disorder, whereas $\tau = 3.3 \cdot 10^4$ for columnar defects, see Table I. This confirms that enhanced thermal fluctuations at elevated temperatures resist the straightening of flux lines as they attempt to bind to columnar defects; in stark contrast, thermal effects facilitate line roughening when vortices become pinned to uncorrelated point-like disorder.

We also analyzed the effects of a sudden drop in temperature, where we reduced the system's ambient tem-

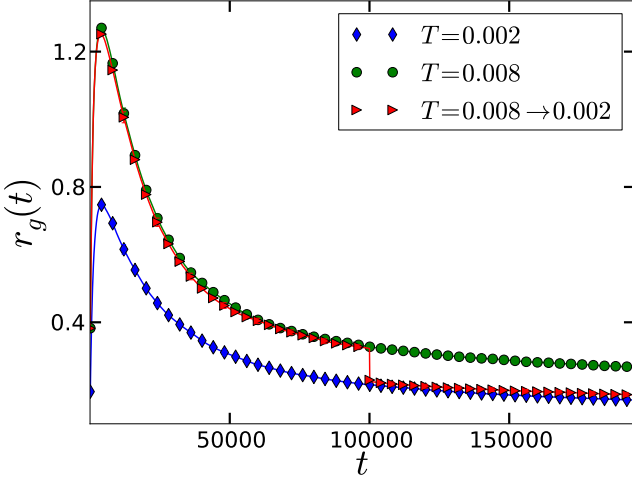


FIG. 4: (Color online) Relaxation of the gyration radius in a system of interacting vortex lines with columnar pinning centers, when the temperature is held fixed or instantaneously lowered (data averaged over 1000 realizations).

perature at $t = 10^5$ from $T = 0.008$ to $T = 0.002$ in our simulation runs. The subsequent vortex relaxation kinetics displays some noticeable differences as compared with the previous up-quenches: Following the temperature decrease, the gyration radius decreases and the fraction of pinned line elements increases in samples with both types of disorder, and non-monotonic behavior is observed in neither of these quantities, as depicted for r_g in Fig. 4. When the temperature suddenly drops, more line elements simply become pinned to either point-like or extended defects, which causes a concomitant decrease in the transverse spatial fluctuations of the vortex lines.

IV. MAGNETIC FIELD QUENCHES

A. Non-interacting Vortex Lines without Disorder

We now proceed to study the effects of sudden changes in the external magnetic field, *i.e.*, vortex density, while keeping the ambient temperature fixed at $T = 0.002$ in all simulation runs for the various systems described in this section. The dynamics of non-interacting directed lines in the absence of disorder can be directly mapped to the one-dimensional Edwards-Wilkinson interface growth model (which is in turn equivalent to a free noisy diffusion equation). The two-time height-height autocorrelation function (5) in the correlated regime is found to be [40]

$$C(t, s) = C_0 s^{1/2} \left(\left[\frac{t}{s} + 1 \right]^{1/2} - \left[\frac{t}{s} - 1 \right]^{1/2} \right). \quad (8)$$

Indeed, if a simple aging scenario applies, one expects the general scaling form for the height-height autocorrelation

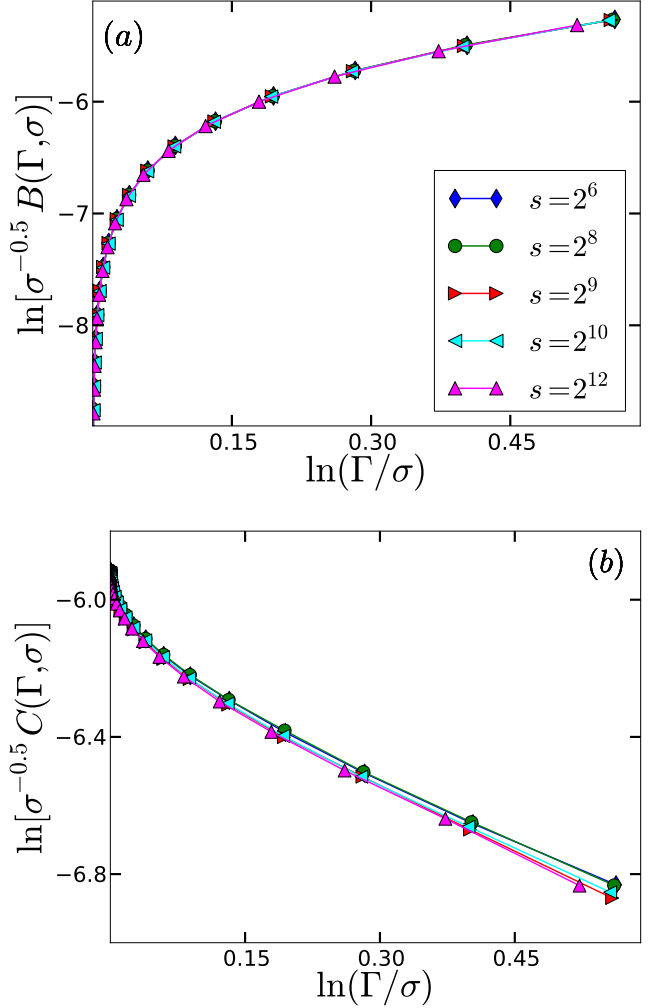


FIG. 5: (Color online) Relaxation of (a) the mean-square displacement and (b) the height-height autocorrelation function for non-interacting vortices in the absence of disorder and for fixed vortex density (data averaged over 800 realizations).

function [25]

$$C(t, s) = s^b f_C(t/s) \quad (9)$$

with a scaling function f_C . In the free diffusive Edwards-Wilkinson regime, the scaling exponent is $b = 1/2$ [31, 40]. In our Langevin molecular dynamics study, we first analyze this case of free non-interacting vortex lines and start with the fixed magnetic field scenario to validate our numerical code. The two-time mean-square displacement (6) follows a similar scaling form to (9). As shown in Fig. 5, our data for both $B(\Gamma, \sigma)$ and $C(\Gamma, \sigma)$ indeed satisfy dynamical scaling for all explored waiting times with the predicted scaling exponent $b = 1/2$, after properly accounting for the long initial relaxation time r , see Sec. II D.

When we follow our magnetic field quench scenario, and suddenly reduce the vortex density after letting the system relax for an extended time period, we obtain

the very same relaxation results for both $B(\Gamma, \sigma)$ and $C(\Gamma, \sigma)$, which is to be expected since the lines are not interacting.

Similarly, when we instantaneously increase the magnetic field, $B(\Gamma, \sigma)$ and $C(\Gamma, \sigma)$ measured for those vortices that were present initially are not significantly different from those quantities obtained at fixed flux density, as the relaxation processes for these non-interacting vortex lines are statistically the same in both situations. However, the subpopulation of newly added lines displays a similar, but less perfect collapse for $C(t, s)$ than that displayed in Fig. 5b since these lines were not present for the previous long relaxation time r , and thus are not yet as relaxed as the initial lines. On the other hand, $B(t, s)$ obtained just for the added lines exhibits perfect dynamical scaling with the scaling exponent $b = 1/2$.

In summary, we confirm the expected Edwards-Wilkinson aging scaling for the non-equilibrium relaxation dynamics of non-interacting flux lines in the absence of disorder, regardless of sudden changes in their density. The following subsections highlight the effects of disorder on the relaxation dynamics of non-interacting, thus statistically independent vortex lines.

B. Non-interacting Flux Lines with Point Disorder

Keeping the repulsive vortex-vortex interactions switched off, we now introduce point defects into the system to study the effects of this type of spatially uncorrelated disorder on the relaxation dynamics.

First, we consider the situation of fixed magnetic field (vortex density), and study the same dynamical quantities as in the previous section, see also Refs. [31, 32]. The mean-square displacement $B(\Gamma, \sigma)$ does not display dynamical scaling with $b = 1/2$ as in the disorder-free case.

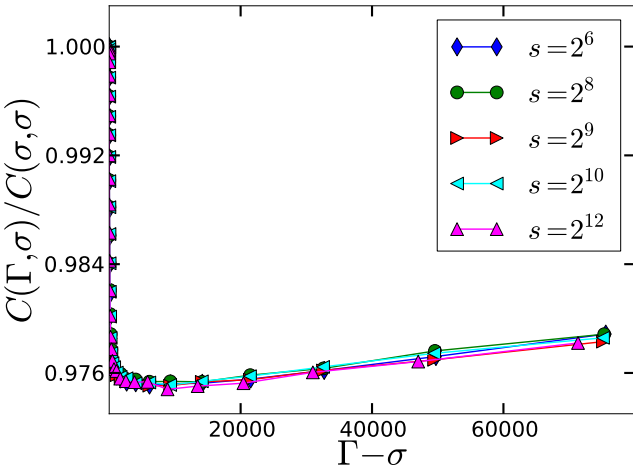


FIG. 6: (Color online) Relaxation of the normalized height-height autocorrelation function in a system of non-interacting flux lines subject to point-like disorder, when the number of flux lines stays fixed (data averaged over 800 realizations).

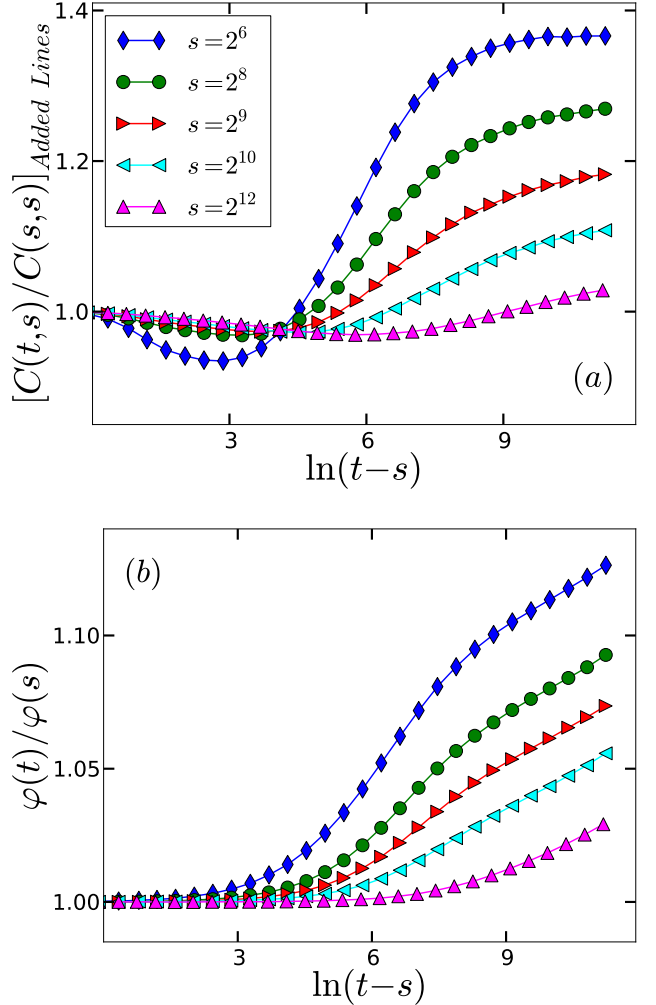


FIG. 7: (Color online) Relaxation of (a) the normalized height-height autocorrelation function of the newly added flux lines, and (b) the fraction of pinned line elements in a system of non-interacting vortices subject to point disorder, following a sudden increase in the magnetic field or vortex density (data averaged over 800 realizations).

Instead, dynamical scaling ensues for $B(\Gamma, \sigma)$ with the aging exponent $b \approx 0.725$, *c.f.* Fig. 6(d) in Ref. [32]. In contrast, dynamical scaling is not observed for the height-height autocorrelation function $C(\Gamma, \sigma)$. As shown in Fig. 6, the data for all waiting times s display identical time evolution, since the system has in fact fully equilibrated owing to the long relaxation period $r = 10^5$, and time translation invariance is restored. The height autocorrelation function shows a similar increase for all waiting times indicating that flux line elements keep exploring their surroundings in search of favorable pinning sites, which causes the lines to continuously roughen due to the uncorrelated nature of the point-like disorder in the system.

The results for a sudden magnetic field decrease (vortex density down-quench) turn out to not significantly

differ from the situation with constant field. This is readily attributed to the fact that the lines are not interacting, and thus the remaining vortices after the quench are not at all affected by the removal of some lines from the sample.

More distinct features are observed upon an instantaneous increase of the magnetic field: First of all, the mean-square displacement $B(\Gamma, \sigma)$ of the initial lines does not display dynamical scaling anymore, but the data (not shown) reveal that this vortex subpopulation has rather recovered time translation invariance, since they all collapse onto a single curve when plotted against $\Gamma - \sigma = t - s$, while the added line subpopulation displays neither of these straightforward features. The height-height autocorrelation function $C(\Gamma, \sigma)$ of the initial lines shows time translation invariance, akin to the data in Fig. 6. On the other hand, $C(t, s)$ for the added lines, depicted in Fig. 7a, displays an initial decrease followed by an increase, with the minimum shifted to later $t - s$ values for longer waiting times s . The decrease happens when the added lines start noticing the presence of the pinning centers and become pinned to nearby defects, which decreases their transverse fluctuations. The subsequent increase is caused by the flux lines exploring more of the sample and thus becoming rougher as they optimize their pinning configurations.

Hence, the behavior of the added lines is highly influenced by disorder as demonstrated by their height autocorrelations. A one-time observable that also highlights the effects of the sudden increase in the magnetic field is the fraction of pinned vortex line elements φ . In the presence of point disorder, this fraction as shown in Fig. 7b displays a two-step increase, which can be attributed to the pinning dynamics of the newly added magnetic flux lines, as discussed in the context of Fig. 7a.

C. Non-interacting Vortices with Columnar Pins

We proceed to change the type of pinning centers present in the system to columnar defects, which are linearly extended pinning sites that are simulated as potential wells aligned along the z direction, and compare their effects on the relaxation kinetics of non-interacting vortices to that of uncorrelated point disorder.

We again first hold the magnetic field constant and consider the different two-time correlation functions studied above. The mean-square displacement $B(\Gamma, \sigma)$ is found to display dynamical scaling with the aging exponent $b = 1/2$, similar to Fig. 5a in the absence of disorder. It is worth recalling that when flux lines are completely pinned to columnar defects, their mean-square displacement becomes constant, of the order of b_0 . We therefore conclude that the dynamics of $B(\Gamma, \sigma)$ in the accessible time window is clearly dominated by the still unattached lines in the system. The height-height autocorrelation function $C(\Gamma, \sigma)$ does not display dynamical scaling with any fixed scaling exponent. However, when considering

the normalized $C(\Gamma, \sigma)$ with respect to the initial value $C(\sigma, \sigma)$ as depicted in Fig. 8a, we observe that the data for all different waiting times s perfectly collapse onto a single curve, which indicates that time translation invariance is restored and the system is well equilibrated. Next, we measure the fraction of pinned line elements in the system with columnar defects, see Fig. 8c. The data for different waiting times collapse onto a single graph, where the fraction of pinned line elements stays constant for an extended time period and only later, at $\ln(\Gamma - \sigma) \approx 7$, starts increasing. This indicates that $\Gamma \approx 1096 + \sigma$ represents a characteristic time scale when pinning to columnar defects becomes prominent in the system.

When vortices are removed from this system of non-interacting flux lines with columnar defects, the measured mean-square displacement, height autocorrelations, and fraction of pinned line elements all yield identical results to the situation when there is no sudden magnetic field change, as is to be expected in the absence of correlations.

Upon introducing additional flux lines into the system, the mean-square displacement of both the initial and the added lines subpopulations shows dynamical scaling for all waiting times with the same exponent $b = 1/2$ as in the fixed density and field down-quench scenarios. This confirms that sudden changes in the vortex density do not alter the global dynamics of non-interacting flux lines in the presence of columnar defects. The autocorrelation function $C(\Gamma, \sigma)$ for the initially present lines turns out very similar to that at fixed density, see Fig. 8a, whereas the data corresponding to the newly added lines cannot be collapsed according to a simple aging scaling form when plotted against the time ratio t/s . However, the graphs $C(t, s)$ for the added lines for various s do not just fall onto a single curve when plotted against $t - s$, as demonstrated in Fig. 8b. This indicates that this subpopulation of lines is not yet equilibrated for the range of waiting times s employed here. As the additional lines are inserted into the sample, depending on the elapsed waiting time s , they require different time periods t to explore the system and become attached to columnar pins. This is corroborated in the time evolution of the fraction of pinned line elements φ for different waiting times in Fig. 8d, which also does not yield data collapse.

The flux lines present in the sample, especially vortices that were suddenly added to the system, start exploring the surrounding pinning centers sooner for shorter waiting times, whence one observes an earlier increase in the fraction of pinned line elements for smaller s . For the long waiting times in Fig. 8d such as $s = 2^{12}$, the fraction of pinned line elements is fixed at a plateau value for an extended duration because the vortices already had enough time to relax towards favorable configurations after the field up-quench. The increase in $\varphi(t)$ happens at a much later time indicating that the line elements might be migrating between neighboring columnar pinning centers to become pinned to whole defect lines, whereupon their lateral line fluctuations diminish. The overall trend in

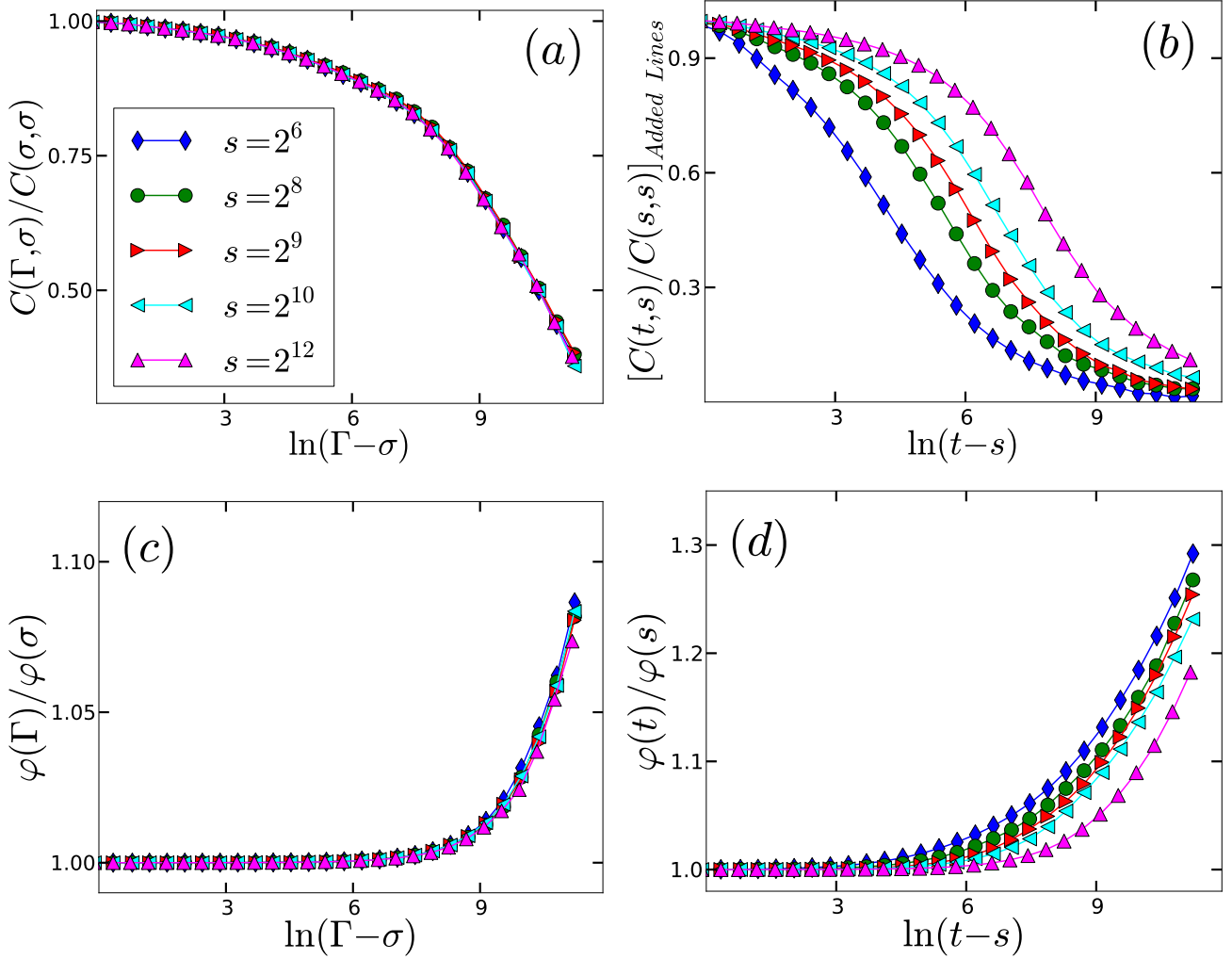


FIG. 8: (Color online) Relaxation of various observables in a system of non-interacting flux lines with columnar defects, (a,c) when the vortex density remains fixed; (b,d) after a sudden increase in the magnetic field: (a,b) normalized height-height autocorrelation function, (c,d) fraction of pinned line elements (data averaged over 800 realizations).

the presence of columnar defects is that the dynamics is dominated by the few lines that remain unattached to any pins, and the tendency of each flux line to become fully localized to a single columnar pinning center, which in turn straightens the vortex lines.

The preceding discussions highlight the influence of different disorder on non-interacting vortex matter and the relaxation dynamics following magnetic field quenches. We expect that quite distinct relaxation kinetics will be observed when mutual vortex interactions are added to our consideration and collective behavior ensues, as will be explored in the following subsections.

D. Interacting Vortex Lines without Disorder

We start with the system of interacting flux lines without disorder. At a fixed magnetic field, we observe at least approximate dynamical scaling of $B(\Gamma, \sigma)$ as dis-

played in Fig. 9a, yet with a different exponent $b = 1.57$ from before. On the other hand, the height-height autocorrelation function in Fig. 9b shows a distinct two-step relaxation behavior, where a β relaxation with almost no changes in $C(\Gamma, \sigma)$ is followed by a very slow decay. This is referred to as α - β relaxation scenario, a characteristic feature of structural glasses [31, 41]. Furthermore, a local maximum in $C(\Gamma, \sigma)$ is observed for all waiting times s , which we attribute to the decay of metastable kink configurations. Such single kinks are step-like flux line structures that are stabilized by the screened logarithmic repulsive forces; hence they constitute interaction-induced features that are long-lived. The mean-square displacement $B(\Gamma, \sigma)$ loses the dynamical aging scaling property when lines are removed from the system, whereas $C(\Gamma, \sigma)$ displays similar behavior to that at fixed magnetic field, but with the local maxima absent for most waiting times. This indicates a destabilization of single-kink structures due to the decrease in the number of lines in the sam-

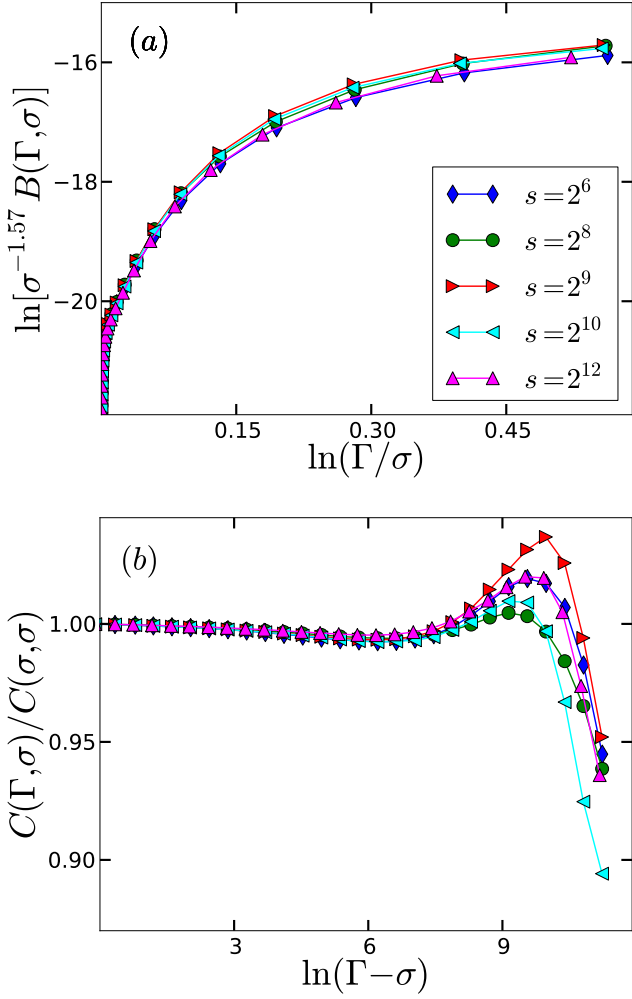


FIG. 9: (Color online) Relaxation of (a) the mean-square displacement and (b) the normalized height-height autocorrelation function in a system of interacting flux lines in the absence of disorder, when the number of flux lines stays fixed (data averaged over 800 realizations).

ple, which relieves the effective mutual cages generated by the repulsive interactions.

On the other hand, when the magnetic field is suddenly increased and vortices are added to the system, we observe the same time evolution in the mean-square displacement of the added lines, the initial lines, and all the lines combined. The data corresponding to all waiting times collapse onto a single curve with a long-time algebraic growth with the aging scaling exponent $b = 0.1$, see Fig. 10a. This dynamical scaling is manifest only when the initial relaxation time r is disregarded in our scaling formula for both the initial lines and the collection of all lines. The independence of these subpopulations from the initial relaxation time implies that the respective lines do not retain memory of their early dynamics and only experience changes upon the addition of new vortices, reflecting the mutual interactions and consequent dynamical correlations.

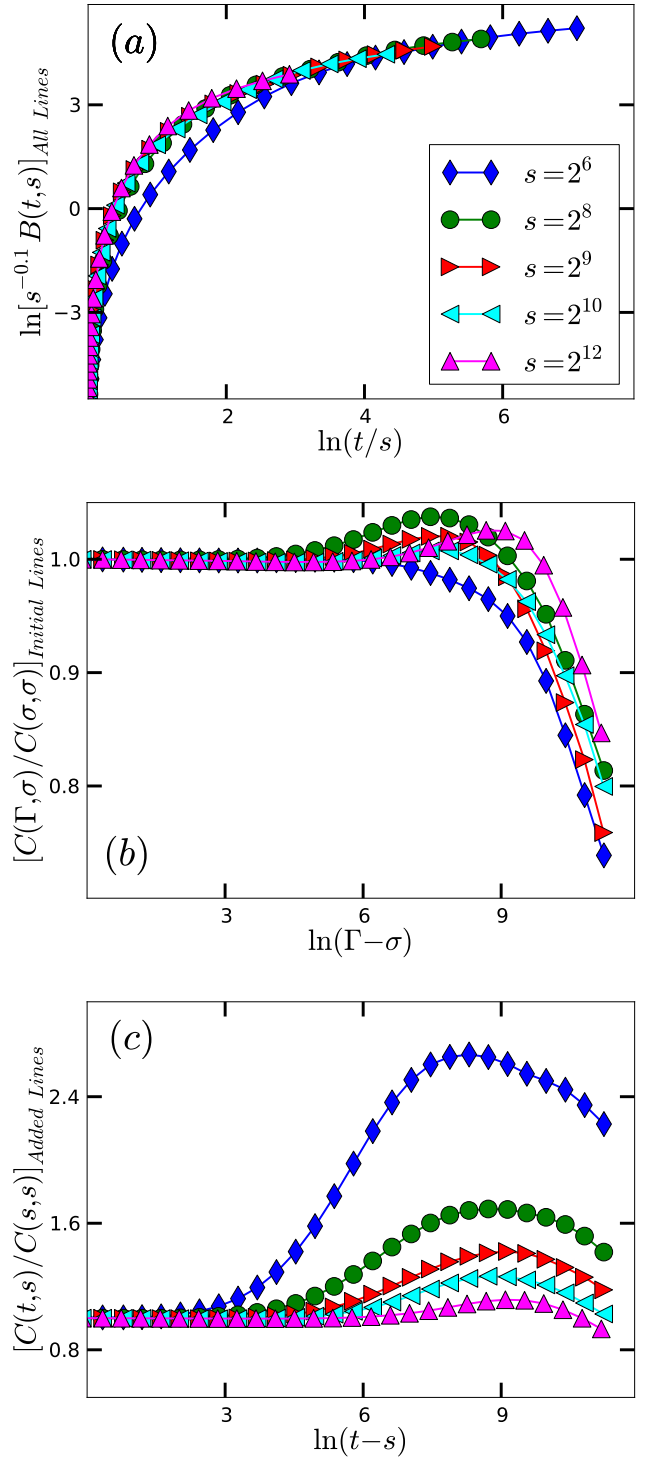


FIG. 10: (Color online) Relaxation of (a) the mean-square displacement of all the flux lines combined, the normalized height-height autocorrelation function of (b) the initially present vortices, and (c) the newly added lines in a system of interacting flux lines in the absence of disorder, following a sudden increase in the magnetic field (data averaged over 900 realizations).

We observe a more diverse temporal evolution in the height-height autocorrelation functions. The initial lines in Fig. 10b show α - β relaxation for all waiting times s with the presence of local maxima similar to those in Fig. 9b. The data display a rather complicated dependence on the sequence of waiting times, which we cannot explain in detail but attribute to the rich and complex nature of the combined vortex system when these initially present and largely relaxed flux lines interact with newly added straight ones. Unlike the initial line subpopulation, the added vortex kinetics presented in Fig. 10c displays a plateau followed by an increase, which is in turn followed by a final decrease for all waiting times. The first increase indicates the time scale when the added lines start noticing the repulsive effect of the already existing vortices, whence lateral fluctuations are enhanced. At later times following this initial increase, $C(t, s)$ decreases again indicating that the lines have reached a steady state with well-established mutual interaction cages, and hence their fluctuations become reduced.

In the following subsections, we investigate and analyze the effects of disorder on samples of interacting vortex lines. We first address uncorrelated point-like defects and then proceed to extended columnar pins.

E. Interacting Flux Lines with Point Disorder

Considering first the case when the magnetic field does not suddenly change, our sample of interacting lines in the presence of point disorder shows dynamical scaling for $B(\Gamma, \sigma)$ with the aging exponent $b = 1.54$, similar to the scaling behavior displayed in Fig. 9a in the disorder-free interacting vortex system. This similarity suggests that the strong repulsive forces between the flux lines dominate over the effects of point-like pinning centers, which do not play a significant role in modifying the global relaxation dynamics of interacting vortices. Even though the height-height autocorrelation function does not show dynamical scaling, the data for the different waiting times collapse onto a single curve indicating that the system has effectively equilibrated, see Fig. 11a. The fraction of the pinned line elements $\varphi(t)$ depicted in Fig. 11c too shows evidence for equilibration for all waiting times considered in our simulations. The data display a plateau followed by an increase in the pinned line element fraction at $\ln(\Gamma - \sigma) \approx 7$, which coincides with the time of marked decrease in $C(\Gamma, \sigma)$, confirming that $\Gamma \approx 1096 + \sigma$ represents a characteristic temporal scale when pinning to point-like defects causes significant flux line roughening.

When flux lines are suddenly removed from the system, $B(\Gamma, \sigma)$ of the remaining lines does not display dynamical scaling. Moreover, $C(\Gamma, \sigma)$ in Fig. 11b still shows the α - β relaxation scenario for all waiting times without the system ever becoming fully equilibrated as in Fig. 11a. The fraction of pinned line elements undergoes a more diverse temporal evolution for the different waiting times, as can be observed in Fig. 11d. For short waiting times $s \leq 2^8$,

a minimum in φ occurs at $\ln(\Gamma - \sigma) \approx 6.2$. The initial decrease indicates that the sudden release of caging due to removed lines leads to depinning of some remaining vortices from point defects where the line elements were only held in place because of their interactions with the removed lines. This enables the remaining flux lines to explore a farther range of their surroundings, ultimately becoming bound to new and more point pins to eventually reach a steady-state fraction φ that is a little larger than the initial one. For intermediate-to-larger waiting times $s > 2^9$, this minimum in the pinned line element fraction is not visible and the data looks similar to the situation with fixed vortex density, see Fig. 11c; the only difference being that the quenched system has clearly not equilibrated yet.

Let us now explore the effects of a sudden increase in the magnetic field, where new straight flux lines are added to the a previously relaxed system of interacting vortices in the presence of point disorder, and analyze the resulting dynamics. Dynamical scaling of the mean-square displacement is lost for the newly added lines, the initially present vortices, and all the flux lines combined. However, the mean-square displacement as function of time looks similar among all these different subpopulations; an example is shown in Fig. 12a. Note that our choice of a putative aging scaling exponent $b \approx 0.8$ in Fig. 12a is merely to demonstrate the global dynamical evolution of $B(t, s)$ for the different vortex subpopulations.

On the other hand, the height-height autocorrelation function shows similar results for the initial lines and the combination of all vortices, as shown in Fig. 12b, where α - β relaxation is evident as a characteristic feature in these flux line subpopulations that have already relaxed for a long time period, but are still not equilibrated. This lack of equilibration becomes manifest in the height-height autocorrelation function for just the subpopulation of added lines in Fig. 12c. For these newly introduced vortices, only very long waiting times $s \geq 2^{12}$ display α - β relaxation kinetics comparable to the situation at fixed magnetic field. However, data corresponding to $s < 2^{12}$ show an initial increase in $C(t, s)$ followed by a slow decrease. When new flux lines are inserted into the sample, the originally present vortices repel them and thus facilitate their pinning to the uncorrelated point disorder, which enhances transverse line fluctuations. At $\ln(t - s) \approx 7$, the added lines' height autocorrelation function decreases because the lines have found a (near) optimal pinning configuration. The fraction of pinned line elements behaves analogously to that in the case of a sudden vortex density decrease, Fig. 11d, with the mere difference that the minimum is less pronounced for a sudden magnetic field up-quench. Yet in this case, the sudden presence of additional caging potentials (rather than their release) and subsequent vortex rearrangement leads to the observed behavior of the pinned line element fraction.

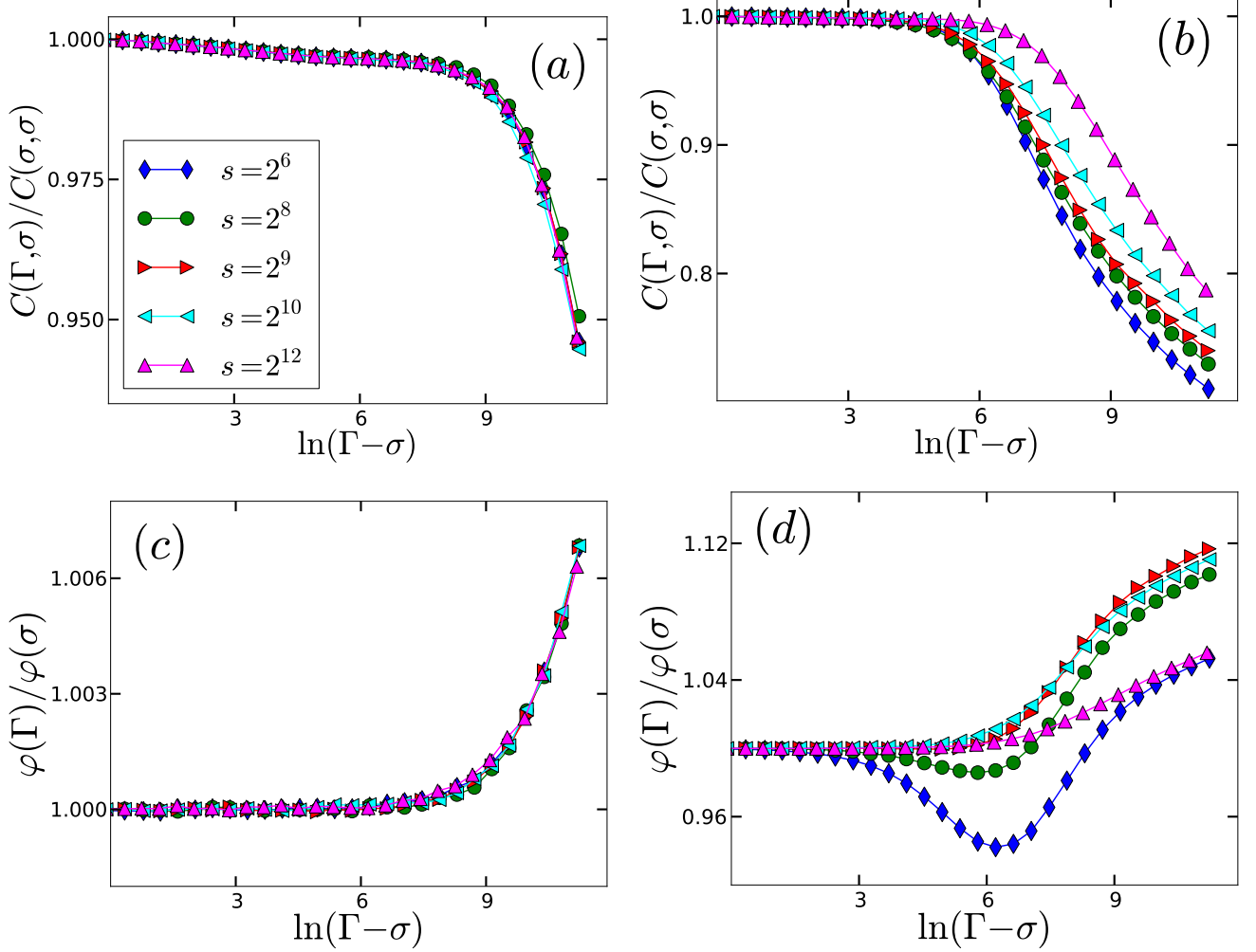


FIG. 11: (Color online) Relaxation of various observables in a system of interacting flux lines with point-like disorder when (a,c) the vortex density remains fixed, and (b,d) after a sudden magnetic field decrease: (a,b) normalized height-height autocorrelation function, (c,d) fraction of pinned line elements (data averaged over 800 realizations).

F. Interacting Vortices with Columnar Defects

Finally, we analyze a sample of interacting flux lines in the presence of columnar defects, and compare the relaxation kinetics in this system with the preceding investigation of uncorrelated point disorder.

We first study the case when the magnetic field stays constant. We find that $B(t, s)$ shows dynamical scaling at long times with the aging scaling exponent $b = 0.8$, see Fig. 13. In contrast, no dynamical scaling is obtained for $C(\Gamma, \sigma)$ which displays a time evolution similar to that in Fig. 11a for point defects. The fraction of pinned line elements in the presence of columnar defects turns out to not significantly differ from that in the presence of point disorder at fixed vortex density.

When flux lines are removed from the sample, dynamical scaling is not observed for $B(\Gamma, \sigma)$, even at long times. Furthermore, time translation invariance in the normalized height-height autocorrelation function indicates an

essentially equilibrated system that undergoes α - β relaxation. This behavior is accompanied by an increasing fraction of pinned line elements confirming that the remaining flux lines undergo similar relaxation dynamics as in the system at fixed magnetic field, namely a continuous straightening and hence reduced transverse fluctuations as the vortices find nearby columnar pinning centers.

Quite different features are observed when the magnetic field is increased instantaneously: The temporal growth of the mean-square displacement $B(t, s)$ of the newly introduced lines looks similar to samples with point-like disorder as shown in Fig. 12a. The similarity in the mean-square displacement in the presence of both point and columnar pinning sites underscores our earlier observation that introducing disorder into the interacting vortex system has comparatively little effect on the global dynamics which is highly dominated by the strong repulsive forces between the flux lines. Analogous to the case when point disorder is present, all the dif-

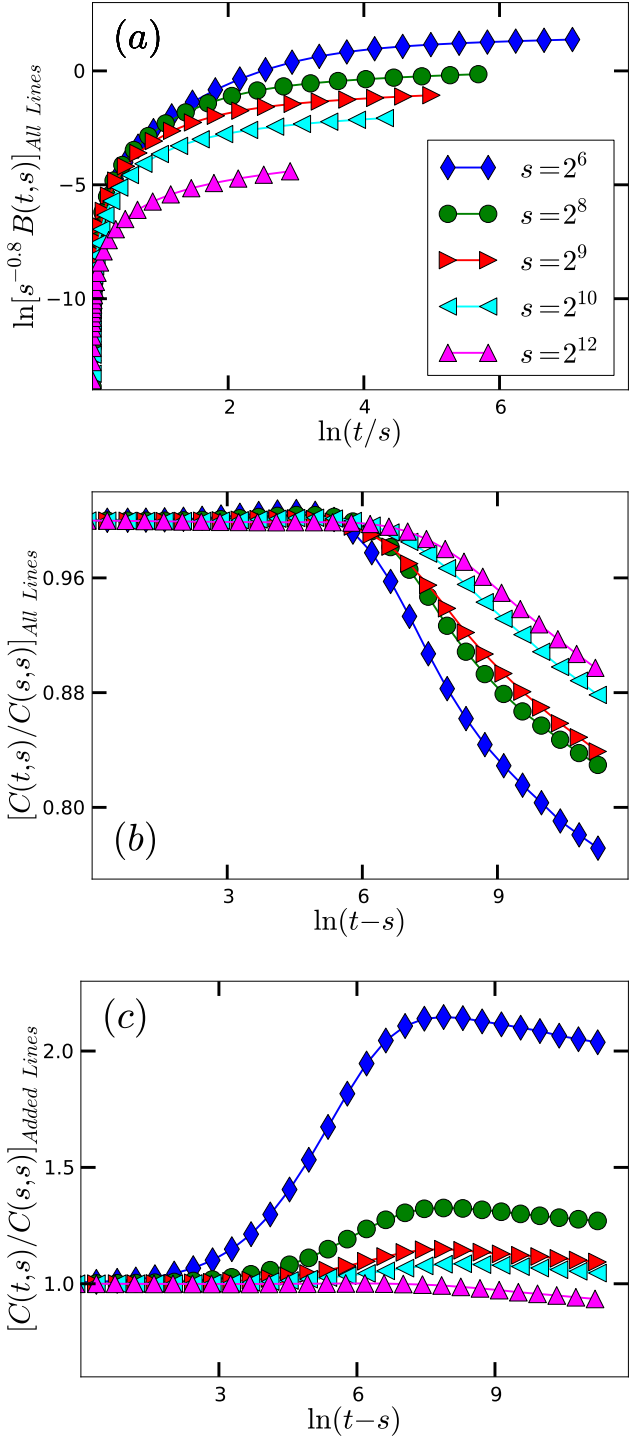


FIG. 12: (Color online) Relaxation of (a) the mean-square displacement, the normalized height-height autocorrelation function (b) of all the flux lines combined, and (c) of the subpopulation of newly added lines in a system of interacting vortices subject to point disorder, following a sudden increase in the magnetic field (data averaged over 800 realizations).

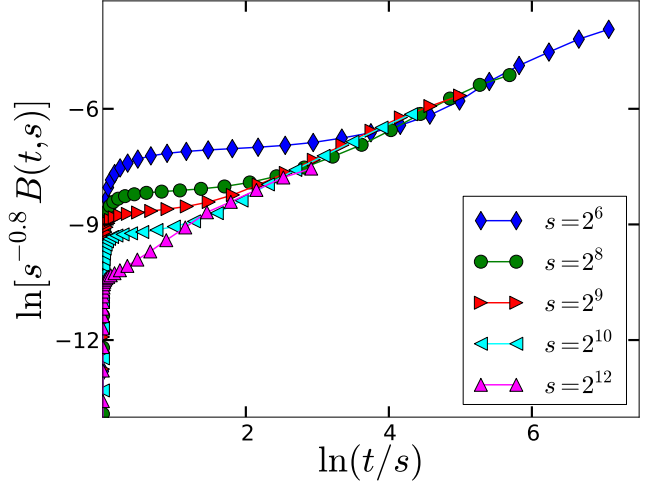


FIG. 13: (Color online) Relaxation of the mean-square displacement in a system of interacting flux lines with columnar defects, when the vortex density remains fixed (data averaged over 1500 realizations).

ferent vortex subpopulations show similar results for the mean-square displacement.

On the other hand, the added vortices and the initially present flux lines are characterized by different height autocorrelations. The initial vortices as well as the combination of all lines display α - β relaxation for all waiting times s . The appearance of local maxima for some long waiting times indicate the decay of long-lived vortex double kinks in the system. However, the subpopulation of added lines displays different features in their height autocorrelations $C(t,s)$ for the different waiting times, see Fig. 14a. For short waiting times, *e.g.* $s = 2^6$, an initial decrease is followed by a pronounced maximum in $C(t,s)$. The initial decrease is set by the time scale when the added flux lines begin to notice the pinning centers, causing their local transverse fluctuations to decrease. The following increase indicates the characteristic time range when the additional vortices start feeling the repulsive interactions with the initially present flux lines and with one another; this produces enhanced fluctuations about their mean lateral positions. This increase continues until pinning effects start to again dominate the relaxation dynamics, rendering the lines straighter and thus reducing vortex line fluctuations. For longer waiting times, α - β relaxation becomes more prominent, with small local maxima present for waiting times $s = 2^8$ and $s = 2^9$. Moreover, the fraction of pinned line elements in Fig. 14b shows an increase followed by asymptotic saturation for all waiting times tested in our simulations.

V. CONCLUSION AND OUTLOOK

In this paper, we have explored the effects of incorporating experimentally motivated initial conditions into

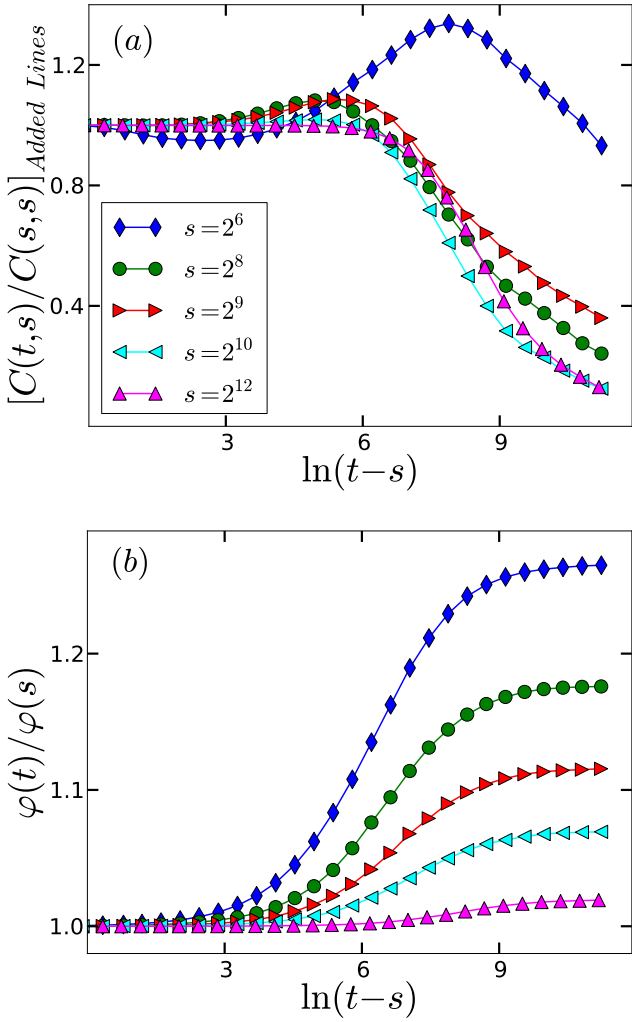


FIG. 14: (Color online) Relaxation of (a) the normalized height-height autocorrelation function of the newly added flux lines, and (b) the fraction of pinned line elements in a system of interacting vortices with columnar defects, following a sudden increase in the magnetic field (data averaged over 800 realizations).

the study of the non-equilibrium relaxation dynamics of magnetic flux lines in type-II superconductors. Random initial conditions were considered in our earlier work in Refs. [31, 32]. In the present study, we focused on the effects of sudden changes in temperature and magnetic field on the ensuing vortex relaxation properties. We investigated the differences between the relaxation kinetics of flux lines in the presence of uncorrelated point-like disorder and columnar defects. To this end, we modeled the magnetic vortices as directed elastic lines and employed a Langevin molecular dynamics algorithm to simulate the vortex kinetics.

We studied the relaxation of a system of interacting flux lines in the presence of disorder at fixed temperatures to confirm that higher temperatures induce enhanced thermal fluctuations that counteract the straight-

ening of the vortex lines caused by their pinning to columnar defects, while in contrast these same fluctuations help lines to roughen when binding to uncorrelated point-like disorder. Furthermore, we investigated the relaxation processes following sudden changes in the ambient temperature. Systems subject to the two types of disorder show very distinct relaxation dynamics when the temperature is instantaneously increased due to the different (de-)pinning behavior from these defects. Some flux line elements become depinned from the uncorrelated point defects following a sudden increase in the sample's temperature confirming that this type of disorder enhances the thermal wandering of flux lines. However, samples with columnar defects display a non-monotonic behavior in spatial fluctuations due to the creation and subsequent decay of vortex double-kinks. These pronounced differences between systems with point-like and columnar defects are not present when the temperature is suddenly reduced, since this decrease simultaneously binds more line elements to the pinning centers, regardless of the type of disorder present in the sample.

We carefully investigated the effects of sudden changes in the magnetic field, *i.e.*, vortex density, on the relaxation processes of flux lines, and performed a systematic analysis to disentangle the contributions of the repulsive vortex-vortex interactions and pinning to the distinct point-like and columnar defects. We compared the cases when the magnetic field instantaneously increases or decreases to the situation when it stays fixed. We start with perfectly straight and randomly placed vortex lines and let the system relax for an extended relaxation time period, after which we maintain a fixed number of lines representing a constant magnetic field. Alternatively, we remove randomly selected lines from the initially relaxed vortices in the sample, or add perfectly straight new flux lines at random positions into the system of relaxed lines, to analyze the effects of a sudden decrease or increase in the magnetic field, respectively.

We validated our numerical studies by showing that our results for free, non-interacting vortex lines agree with the analytical predictions from the Edwards-Wilkinson interface growth model. We then introduced point-like and columnar pinning centers to a system of non-interacting flux lines. We found that the relaxation features in samples with columnar disorder are quite similar to the case when no disorder is present, especially in the behavior of global observables, as *e.g.*, visible in the dynamical scaling of the vortex mean-square displacement. This similarity indicates that the dynamics of vortex lines in the presence of columnar disorder is strongly dominated by the still unattached lines in the system. In the three studied cases without vortex interactions, sudden removal of flux lines results in the remaining lines showing similar relaxation behavior to the situation with a fixed vortex density, as expected since caging effects due to the repulsive vortex-vortex interactions are absent. On the other hand, when additional lines are introduced to these systems, the initially existing lines and the added

lines show quite distinct features in their relaxation dynamics.

Thereafter, we added the repulsive screened logarithmic interactions into our consideration of systems without disorder, with uncorrelated point-like, or with extended columnar defects. Sudden decreases in the magnetic field result in the remaining lines displaying relaxation properties that differ from the situation when the magnetic field stays fixed, which confirms that caging effects due to vortex-vortex interactions constitute a prominent factor that highly affects the results of sudden changes in the magnetic field. Collective interaction effects are markedly enhanced when accompanied with disorder following sudden increases in the magnetic field, where the relaxation properties of the added lines clearly depend on the type of pinning centers. Point-like disorder enhances transverse spatial vortex line fluctuations by binding each to many pinning centers at once in the vortex glass phase, while columnar defects pin entire flux lines and straighten them in the distinct Bose glass phase. It is worth noting that when comparing the novel results in this paper to our earlier study in Ref. [32] with random initial conditions, we discovered improved dynamical scaling in the vortex mean-square displacement in all situations considered here. Consequently, the currently utilized more realistic initial conditions help the system

to equilibrate faster and thus acquire universal features.

Temperature or magnetic field quenches and the subsequent measurement of one-time observables and two-time correlation functions could be utilized to formulate experimental methods to characterize material samples by means of the observed fluctuation spectrum. In future work, we plan to extend our study to include the effects of driving currents on the transient properties of driven flux line systems, where relaxation towards non-equilibrium steady states will ensue in contrast to the presently analyzed relaxation towards thermal equilibrium. A more detailed understanding of relaxation processes and the origin of deviation from scaling requires identifying the characteristic length scales in the system and their temporal growth, which we hope to pursue through the analysis of space-time observables.

Acknowledgments

This research is supported by the U.S. Department of Energy, Office of Basic Energy Sciences, Division of Materials Sciences and Engineering under Award DE-FG02-09ER46613.

[1] For a now classic review, see: G. Blatter, M. V. Feigel'man, V. B. Geshkenbein, A. I. Larkin, and V. M. Vinokur, Rev. Mod. Phys. **66**, 1125 (1994).

[2] W. K. Kwok, J. Fendrich, S. Fleshler, U. Welp, J. Downey, G. W. Crabtree, J. Giapintzakis, Physica B **197**, 579 (1994).

[3] M. P. A. Fisher, Phys. Rev. Lett. **62**, 1415 (1989).

[4] M. V. Feigel'man, V. B. Geshkenbein, A. I. Larkin, and V. M. Vinokur, Phys. Rev. Lett. **63**, 2303 (1989).

[5] T. Nattermann, Phys. Rev. Lett. **64**, 2454 (1990).

[6] D. S. Fisher, M. P. A. Fisher, and D. A. Huse, Phys. Rev. B **43**, 130 (1991).

[7] W. K. Kwok, S. Fleshler, U. Welp, V. M. Vinokur, J. Downey, G. W. Crabtree, M. M. Miller, Phys. Rev. Lett. **69**, 3370 (1992).

[8] T. Giamarchi and P. Le Doussal, Phys. Rev. Lett. **72**, 1530 (1994).

[9] T. Giamarchi and P. Le Doussal, Phys. Rev. B **52**, 1242 (1995).

[10] J. Kierfeld, T. Nattermann, and T. Hwa, Phys. Rev. B **55**, 626 (1997).

[11] D. S. Fisher, Phys. Rev. Lett. **78**, 1964 (1997).

[12] T. Giamarchi and P. Le Doussal, Phys. Rev. B **55**, 6577 (1997).

[13] For a review, see: T. Nattermann and S. Scheidl, Adv. Phys. **49**, 607 (2000).

[14] D. R. Nelson, Phys. Rev. Lett. **60**, 1973 (1988).

[15] D. R. Nelson and H. S. Seung, Phys. Rev. B **39**, 9153 (1989).

[16] D. R. Nelson, J. Stat. Phys. **57**, 511 (1989).

[17] P. Yang, C. M. Lieber, Science **273**, 1836 (1996).

[18] D. R. Nelson and V. M. Vinokur, Phys. Rev. Lett. **68**, 2398 (1992).

[19] I. F. Lyuksyutov, Europhys. Lett. **200**, 273 (1992).

[20] D. R. Nelson and V. M. Vinokur, Phys. Rev. B **48**, 13060 (1993).

[21] M. P. A. Fisher, P. B. Weichman, G. Grinstein, and D. S. Fisher, Phys. Rev. B **40**, 546 (1989).

[22] U. C. Täuber and D. R. Nelson, Phys. Rep. **289**, 157 (1997); e: **296**, 337 (1998).

[23] L. Civale, A. D. Marwick, T. K. Worthington, M. A. Kirk, J. R. Thompson, L. Krusin-Elbaum, Y. Sun, J. R. Clem, and F. Holtzberg, Phys. Rev. Lett. **67**, 648 (1991).

[24] L. C. E. Struik, *Physical Aging in Amorphous Polymers and Other Materials* (Elsevier, Amsterdam, 1978).

[25] M. Henkel and M. Pleimling, *Nonequilibrium Phase Transitions Volume 2 – Ageing and Dynamical Scaling far from Equilibrium* (Springer, Heidelberg, 2010).

[26] M. Henkel, M. Pleimling, and E. Sanctuary, eds., *Ageing and the Glass Transition, Lecture Notes in Physics* **716** (Springer, Berlin, 2007).

[27] X. Du, G. Li, E. Y. Andrei, M. Greenblatt, and P. Shuk, Nat. Phys. **3**, 111 (2007).

[28] E. L. Papadopoulou, P. Nordblad, Svendlindh, S. Schöneberger, and R. Gross, Phys. Rev. Lett. **82**, 173 (1999).

[29] S. Bustingorry, L. F. Cugliandolo, and D. Domínguez, Phys. Rev. Lett. **96**, 027001 (2006).

[30] S. Bustingorry, L. F. Cugliandolo, and D. Domínguez, Phys. Rev. B **75**, 024506 (2007).

[31] M. Pleimling and U. C. Täuber, Phys. Rev. B **84**, 174509

(2011).

[32] U. Dobramysl, H. Assi, M. Pleimling, and U. C. Täuber, *Eur. Phys. J. B* **86**, 228 (2013).

[33] D. Vasyukov, Y. Anahory, L. Embon, D. Halbertal, J. Cuppens, L. Neeman, A. Finkler, Y. Segev, Y. Myasoedov, M. L. Rappaport, M. E. Huber, and E. Zeldov, *Nature Nanotech.* **8**, 639 (2013).

[34] O. M. Auslaender, L. Luan, E. W. J. Straver, J. E. Hoffman, N. C. Koshnick, E. Zeldov, D. A. Bonn, R. Liang, W. N. Hardy, and K. A. Moler, *Nature Phys.* **5**, 35 (2009).

[35] Y. Abulafia, A. Shaulov, Y. Wolfus, R. Prozorov, L. Burlachkov, D. Majer, E. Zeldov, V. M. Vinokur, and Y. Yeshurun, *J. Low Temp. Phys.* **107**, 455 (1997).

[36] J. Das, T. J. Bullard, and U. C. Täuber, *Physica A* **318**, 48 (2003).

[37] T. J. Bullard, J. Das, G. L. Daquila, and U. C. Täuber, *Eur. Phys. J. B* **65**, 469 (2008).

[38] A. Brass and H. J. Jensen, *Phys. Rev. B* **39**, 9587 (1989).

[39] M. M. Abdelhadi and K. A. Ziq, *Supercond. Sci. Tech.* **7**, 99 (1994).

[40] A. Röthlein, F. Baumann, and M. Pleimling, *Phys. Rev. E* **74**, 061604 (2006).

[41] W. Götze and L. Sjogren, *Rep. Prog. Phys.* **55**, 241 (1992).